ACS OMEGA

Open Access
This article is licensed under CC-BY-NC-ND 4.0

http://pubs.acs.org/journal/acsodf
Article

Solubility Change Behavior of Fluoroalkyl Ether-Tagged Dendritic Hexaphenol under Extreme UV Exposure

Hyun-Taek Oh,[▽] Gayoung Kim,[▽] Seok-Heon Jung, Yejin Ku, Jin-Kyun Lee,* Kanghyun Kim, Byeong-Gyu Park, Sangsul Lee, Chawon Koh, Tsunehiro Nishi, and Hyun-Woo Kim

Cite This: *ACS Omega* 2024, 9, 37365–37373

Read Online

ACCESS | Metrics & More | Article Recommendations | Supporting Information

ABSTRACT: This study focuses on the discovery of a single-component molecular resist for extreme ultraviolet (EUV) lithography by employing the ionizing radiation-induced decomposition of carbon−fluorine chemical bonds. The target material, **DHP-L6**, was synthesized by bonding perfluoroalkyl ether moieties to amorphous dendritic hexaphenol (DHP) with a high glass transition temperature. Upon exposure to EUV and electron beam irradiation, **DHP-L6** films exhibited a decreasing solubility in fluorous developer media, resulting in negative-tone images. The underlying chemical mechanisms were elucidated by Fourier transform-infrared spectroscopy (FT-IR), X-ray photoelectron spectroscopy, and nanoindentation experiments. These analyses highlighted the possible electron-induced decomposition of C−F bonds in **DHP-L6**, leading to molecular network formation via recombination of the resulting C-centered radicals. Subsequent high-resolution lithographic patterning under EUV irradiation showed that **DHP-L6** could create stencil patterns with a line width of 26 nm at an exposure dose of 110 mJ cm^{-2}. These results confirm that single-component small molecular compounds with fluoroalkyl moieties can be employed as patterning materials under ionizing radiation. Nonetheless, additional research is required to reduce the relatively high exposure energy for high-resolution patterning and to enhance the line-edge roughness of the produced stencil.

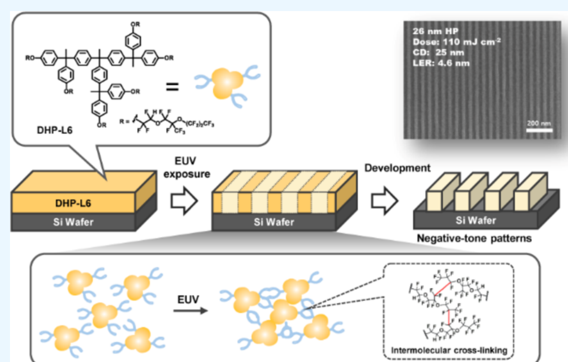

1. INTRODUCTION

Emerged though Kilby's pioneering work in the late 1950s and now central to the application of artificial intelligence, high-performance semiconductor integrated circuit (IC) chip technologies encompass both virtual circuit design and microfabrication in the real world.[1,2] To develop physical IC chips able to perform calculations faster while consuming less energy, it is crucial to achieve manufacturing processes that maximize the number of components and simultaneously minimize the distance among them within a smaller semiconductor die. Photolithography plays a key role in this process, by adopting photographic techniques to create stencils using a light-sensitive material, known as photoresist (PR).[3,4] Based on Rayleigh's equation, the formation of more finely defined PR stencils are accomplished by utilizing shorter-wavelength light.[5−7] Therefore, the time-consuming, complex multipatterning technique, involving repeated exposure to 193 nm deep ultraviolet (DUV) light, has evolved into a single-exposure protocol, employing 13.5 nm extreme ultraviolet (EUV) light to create structures with critical dimensions (CDs) smaller than 20 nm.

The transition from DUV to EUV light sources requires not only the introduction of new exposure tools, but also advanced PRs. Because EUV lithography (EUVL) operates with a markedly reduced number of photons having significantly higher energy, it is strongly influenced by photon shot-noise effects.[8−10] This leads to deterioration in the quality of the printed PR stencils, particularly in their line-edge roughness (LER). Another potentially serious issue is that, if the stochastic distribution of incident photons interacts synergistically with the chemical inhomogeneity of the film, the quality of the stencils can be further reduced.

Chemically amplified photoresist (CAR) films, employed in traditional DUV lithography and currently applied in EUVL, consist of three main components:[11−13] a polymer resin that makes up the bulk of the resist film with a changing solubility in the developer solution, a photoacid generator (PAG) that produces an acid catalyst during exposure to switch the solubility of the polymer resin, and a base quencher that controls the diffusion of acid molecules and reduces the pattern roughness during the catalytic acidolysis reactions.

Received: June 13, 2024
Revised: August 12, 2024
Accepted: August 14, 2024
Published: August 20, 2024

© 2024 The Authors. Published by American Chemical Society

https://doi.org/10.1021/acsomega.4c05535
ACS Omega 2024, 9, 37365−37373

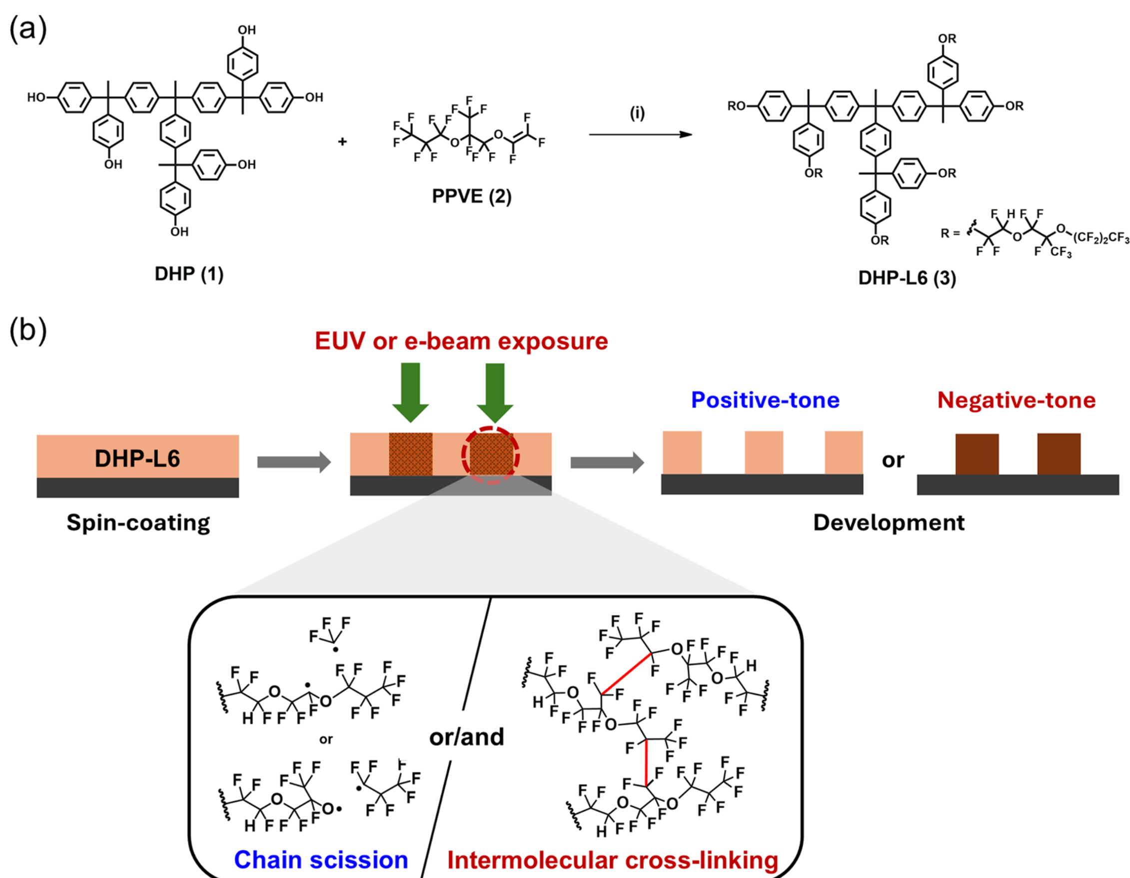

Figure 1. (a) Synthesis of **DHP-L6** (**3**). Reagents and conditions: (i) **DHP** (**1**), **PPVE** (**2**), K_2CO_3, DMF, 70 °C, 2 h. (b) Proposed reaction pathways for forming structures with **DHP-L6** (**3**) under high-energy irradiation.

Polymer chains grow via the stochastic combination of two or more monomers and cease growing through termination or chain-transfer reactions.[14−16] During this process, the resin is composed of chains that exhibit heterogeneity in the composition of their constituent monomers and length. This heterogeneity in the polymer chains, combined with the spatially uneven distribution of the PAG and base quencher within the CAR film, is known to contribute to the quality degradation of stencils. Therefore, the application of EUV resists free from chemical and physical inhomogeneities is a desired goal.

One promising approach to achieving this goal involves developing resist materials based on amorphous organic molecules, or molecular resists, whose solubility changes solely through interactions with EUV photons and the resulting secondary electrons (SEs), without the need for additional components like PAGs or base quenchers. These materials offer advantages in producing higher resolution stencil patterns with smaller LER values, thanks to their smaller molecular size and monodisperse molecular weight distribution compared to polymer-based structures.[17] While most recent research focuses on CAR-type molecular resists, there has been little exploration in the area of non-CAR-type, single-component molecular resists.[18−22] Notably, Yang and Li's group reported a non-CAR-type molecular resist featuring a bis(4-butoxyphenyl)sulfone core chemically bound to four triphenylsulfonium units, which showed promising results in achieving high-resolution, low LER patterns.[23] Given the potential of non-CAR-type molecular resists to perform well under extreme ultraviolet (EUV) light and overcome the limitations of conventional PRs, we explored single-component molecular resists that operate via the unique decomposition pathway of C−F bonds.

In this context, this article reports the development of a homogeneous molecular EUV resist characterized by a single molecular weight, which exploits the distinctive degradation pathway of carbon−fluorine chemical bonds. Six perfluoroalkyl ether moieties were attached to a dendritic hexaphenol core (**DHP** (**1**), Figure 1a) known for its high glass transition temperature (T_g). Subsequently, thin films cast with this material were exposed to EUV light to evaluate the working mechanism and patterning performance of the fluorinated resist.

2. EXPERIMENTAL METHODS

2.1. Materials. *N*,*N*-Dimethylformamide (DMF), propylene glycol monomethyl ether acetate (PGMEA), and 1-methoxy-2-propanol (PGME) were purchased from Sigma-Aldrich. 2-(Heptafluoropropoxy)hexafluoropropyl trifluorovinyl ether (**PPVE**, **2**) and 2-heptanone were bought from TCI Chemicals. All chemicals were used without further drying or purification processes. 3-Ethoxy-1,1,1,2,3,4,4,5,5,6,6,6-dodecafluoro-2-trifluoromethyl-hexane (Novec-7500), perfluorocarbons (FC-3283, FC-770, FC-40), and 1,1,1,2,3,3-hexafluoro-4-(1,1,2,3,3,3 hexafluoropropoxy) pentane (Novec-7600) were purchased from 3 M Korea (Figure S1).

2.2. Characterization. ^{1}H NMR spectra were recorded on a Avance III (400 MHz, Bruker) spectrometer at ambient

https://doi.org/10.1021/acsomega.4c05535
ACS Omega 2024, 9, 37365−37373

temperature using the chemical shift of the residual protic solvent ($CHCl_3$ at δ = 7.24 ppm) as internal reference. All chemical shifts are quoted in parts per million (ppm) relative to the internal reference, and the coupling constants J are measured in Hz. The multiplicity of the signals is indicated as follows: s (singlet), d (doublet), and m (multiplet). Thermogravimetric analysis (TGA, TGA Q50, TA Instruments) measurements were performed by starting at 25 °C and heating to 800 °C at a rate of 10 °C min^{-1} under N_2. Differential scanning calorimetry (DSC, DSC200F3, Netzsch, Germany) measurements were carried out in dry N_2 atmosphere at a flow rate of 10 cm^3 min^{-1}. The sample weight in the DSC experiment was 3.5 mg, and the data were calibrated using indium as a standard. The thermal history of the samples was removed by scanning from 20 to 250 °C at a heating rate of 10 °C min^{-1}, followed by cooling to 20 °C at 10 °C min^{-1}. Attenuated total reflectance (ATR) FT-IR spectra of film-state samples were recorded on a Bruker VERTEX 80 V instrument connected to a Hyperion 2000 microscope. X-ray photoelectron spectroscopy (XPS, PHI 5700 ESCA) experiments were performed using monochromatic Al Kα radiation ($h\nu$ = 1486.6 eV). Nanoindentation tests were performed using a nanoindenter (Nanomechanics) with a continuous stiffness measurement (CSM) technique. EUV exposure experiments were performed at the Pohang Accelerator Laboratory (PAL, Republic of Korea) using the 4A1 beamline of PLS-II accelerator to investigate the solubility change mechanism,[24] and at the Lawrence Berkeley National Laboratory (LBNL), using the MET5 exposure tool operated by CXRO for EUV lithographic patterning. Line and space patterns were observed using high-resolution field emission scanning electron microscopy (FE-SEM) (JSM-7800F Prime, JEOL, Japan) after chemical vapor deposition (CVD) of Os. The LER values of the resist patterns were calculated using the SuMMIT software (EUV Tech Inc.).

2.3. Synthesis of PPVE-Tagged Dendritic Hexaphenol (DHP-L6). **DHP** (**1**) (0.8 g, 0.89 mmol), **PPVE** (**2**) (3.5 g, 8.04 mmol), K_2CO_3 (1.5 g, 10.7 mmol), and DMF (anhydrous, 15 cm^3) were added to a round flask (100 cm^3). The reaction mixture was stirred at 70 °C for 2 h, allowed to cool to ambient temperature, and then quenched by addition of water and EtOAc. The organic layer was separated, washed with water and brine, dried over anhydrous $MgSO_4$, and finally concentrated under reduced pressure. The crude product was purified by column chromatography (silica gel, EtOAc/hexane = 1:5 by volume) to yield white **DHP-L6** (**3**) (2.7 g, 87%). Found: C, 37.77%; H, 1.43%. $C_{110}H_{54}F_{96}O_{18}$ requires C, 37.88%; H, 1.56%; ^{1}H NMR (400 MHz, $CDCl_3$): δ = 7.05 ppm (s, 24H, Ar-H), 6.95 (d, J = 13.0 Hz, 12H, Ar-H), 6.02 (d, J = 54.0 Hz, 6H, CF_2CFHO), 2.13 (s, 12H, CH_3); ^{13}C NMR (100 MHz, $CDCl_3$): δ = 147.08, 147.04, 146.92, 145.69, 129.88, 128.36, 127.94, 120.86, 100−120 (m, CF_2), 51.58, 51.55, 30.54, 30.36; ^{19}F NMR (376 MHz, $CDCl_3$): δ = −145.10 (1F), −144.80 (1F), −129.73 (2F), −86.49 (2F), −85.59 (1F), −83.56 (1F), −81.77 (2F), −81.44 (3F), −80.16 (3F).

2.4. Investigation of Solubility Change Mechanism of DHP-L6 Films under EUV Radiation. *2.4.1. FT-IR and XPS Experiments.* A solution of **DHP-L6** in Novec-7500 was spin-coated on a double-side-polished Si wafer. The coated substrate was then heated at 130 °C for 1 min to form a ca. 300 nm-thick **DHP-L6** film. The latter was exposed to EUV light with energies ranging from 10 to 250 mJ cm^{-2} using an exposure setup installed at the 4A1 beamline of PLS-II accelerator. Without any additional heating, the exposed film was developed for 1 min using FC-3283 liquid, forming circular patterns with a diameter of ca. 220 μm. ATR FT-IR spectroscopy measurements were performed on the residual film patches, with a resolution of 4 cm^{-1} across a wavenumber range of 600 to 4000 cm^{-1}. Prior to XPS analysis, surface contaminants on the patches were removed by sputtering with Ar cluster ions for 15 s. Then, elemental spectra were measured by scanning 5−10 times using an X-ray beam with a spot size of 50 μm.

2.4.2. Nanoindentation Measurements. A 20% (wt/vol) solution of **DHP-L6** in Novec-7500 was used to prepare a thick film specimen. The spin-coated Si substrate was heated at 130 °C for 1 min, resulting in a film of ca. 480 nm thickness on top, and cleaved into several pieces. Each specimen was then exposed to EUV light with energies of 90, 100, 130, 150, and 200 mJ cm^{-2}, separately. Each Si piece was then washed in FC-3283 without an additional baking step. This was followed by nanoindentation measurements to assess changes in the hardness and reduced modulus of the EUV-exposed **DHP-L6** patches using a CSM technique. A Berkovich diamond tip approached the patches at a speed of 100 nm s^{-1} and penetrated them to a depth to 200 nm with a strain rate of 0.05 s^{-1}. The vibration amplitude and frequency of the tip were 2 nm and 100 Hz, respectively. The hardness and reduced modulus of each **DHP-L6** patch were extracted from the data collected at 200 nm penetration depth.

2.5. Lithographic Patterning Evaluation. *2.5.1. Dependence of Dissolution Behavior of **DHP-L6** Films on EUV Exposure Energy.* The experiments were performed using a dose calibration tool at LBNL. A 2.0% (wt/vol) solution of **DHP-L6** in Novec-7500 was spin-coated on a bare Si substrate at 4000 rpm. The coated substrate was then baked at 130 °C for 1 min to form a thin film with a thickness of ca. 40 nm. After EUV exposure with different irradiation energies, the substrate was washed in FC-3283 without any additional thermal annealing steps. Circular patches of insoluble materials derived from **DHP-L6** were observed with an optical microscope. The film thicknesses of the patches were measured using atomic force microscopy (AFM). Then, we plotted the relationship between the remaining film thickness and the EUV exposure energy (the so-called contrast curve).

2.5.2. Patterning Capabilities of DHP-L6 under EUV Lithography Conditions. A 1.5% (wt/vol) solution of **DHP-L6** in Novec-7500 was spin-coated on a bare Si wafer at 3000 rpm. The coated substrate was baked at 130 °C for 1 min to form a ca. 35 nm-thick film. The latter was then exposed to EUV light with energy varying between 74 and 193 mJ cm^{-2}, using the MET5 exposure tool. The development step was carried out in a similar way to the evaluation of the dissolution behavior. The obtained line and space patterns were observed with a high-resolution FE-SEM instrument after chemical vapor deposition of Os for 20 s.

3. RESULTS AND DISCUSSION

EUV is a type of ionizing radiation with an energy of 92 eV, which interacts with the atoms of the resist film, leading them to emit high-energy photoelectrons.[25,26] In turn, these photoelectrons induce the generation of SEs with reduced energy from the resist molecules through electron-impact ionization processes. The SEs break the chemical bonds within the resist molecules via the dissociative electron attachment

https://doi.org/10.1021/acsomega.4c05535
ACS Omega 2024, 9, 37365−37373

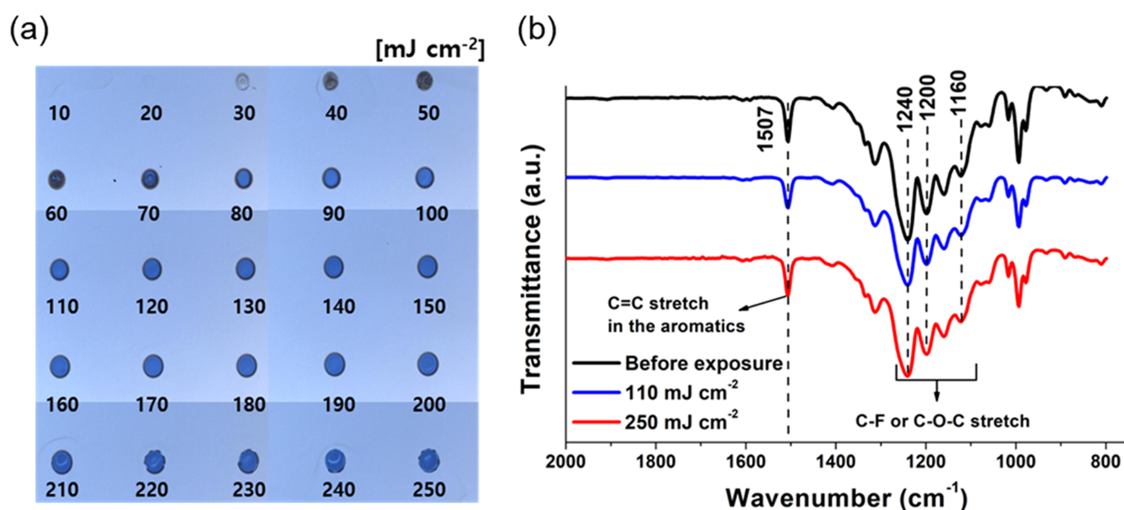

Figure 2. (a) Developed patches of **DHP-L6** generated by exposure to EUV light of energies varying from 10 to 250 mJ cm^{-2} and development step in FC-3283. (b) FT-IR spectra of **DHP-L6** patches obtained by exposure to EUV light with energies of 110 and 250 mJ cm^{-2}.

process, forming carbon-centered radicals.[27,28] The latter then undergo typical radical reactions, including bond scission (β-cleavage) and cross-linking, leading to the formation of stable spin-paired molecules, while at the same time altering the solubility of the resist film (Figure 1b).

In the dissociative electron attachment process, the C−F chemical bond can be considered to dissociate easily. Owing to the higher electronegativity of fluorine, the chemical bond between carbon and fluorine involves depressed bonding (σ) and antibonding (σ^*) orbitals.[29,30] This feature makes the C−F bond highly stable under oxidizing conditions, where electron ejection from the σ orbital is required, and yet vulnerable under reducing conditions, where an electron is introduced into the σ^* orbital, leading to the formation of a C-centered radical. Previous studies showed that the poly(tetrafluoroethylene) (PTFE) undergoes chain-scission or cross-linking reactions between the polymer chains under e-beam and γ-ray irradiation, resulting in changes to its chemical structure and mechanical properties.[31,32] Furthermore, it has been reported that amorphous fluoropolymers, including Teflon AF and Cytop that contain perfluoroalkyl ether linkages, exhibit photodegradation under 157 nm UV light and γ-rays, possibly via radical generation.[33−35]

We were also interested in the specific degradation behavior of the C−F bond and investigated e-beam resist systems based on this phenomenon. Previous experiments confirmed that thin films composed of Cytop, Hyflon AD, and Teflon AF exhibited increased solubility under accelerated e-beam conditions, enabling the formation of nanometer-scale resist patterns (Figure S2). Furthermore, using polymethacrylates possessing perfluoroalkyl side chains, we could examine their degradation and pattern formation behavior under e-beam and EUV lithographic conditions.[36−38]

The fluorinated polymers mentioned above are not e-beam or EUV resists that require separate components, such as a PAG or base quencher, with a spatially inhomogeneous distribution within the film. However, because they are inherently polymers with a molecular weight distribution or a polydispersity index ($Đ$), it would be incorrect to call them single-component electron resists. Even though polymers with a $Đ$ value close to unity were synthesized through the reversible-deactivation radical polymerization technique, the resulting polymer-based resists are still multicomponent materials with both short and long chains mixed together.[39] To remove this inhomogeneity, this study aimed to explore the synthesis and patterning characteristics of e-beam and EUV resist materials characterized by a single molecular weight.

3.1. Material Synthesis and Characterizations. In the first step, we attempted to prepare **DHP** (**1**), which acts as the backbone of the resist molecule and possesses a high thermal degradation temperature (T_d, temperature at which 5% degradation occurs) of 371 °C and a T_g of 130 °C (Figures S3−S5). Previous studies reported the synthesis of **DHP** using a mixture of concentrated HCl and acetic acid to induce electrophilic aromatic substitution reactions between 1,1,1-tris(4-acetylphenyl)ethane and phenol at atmospheric pressure. However, following this protocol, it was found that mainly two of the three acetyl functional groups of 1,1,1-tris(4-acetylphenyl)ethane participated in the reaction with phenol. The desired **DHP** was produced with a low yield of only 11%. The vaporization of HCl (serving as a catalyst) at 90 °C was identified as one of the reasons for this low yield. To address this issue, the synthesis conditions were modified by using concentrated HCl as the sole solvent, while performing the reaction in a pressurized vessel. As a result, the formation of byproducts was significantly reduced, and the yield of **DHP** increased to 45%.

The six phenolic hydroxyl groups present in **DHP** can readily participate in a coupling reaction with **PPVE** (**2**), which contains an electrophilic vinyl moiety (Figure 1a). Using the commonly employed base−solvent combination of K_2CO_3 and DMF, all six phenolic hydroxyl groups in **DHP** were transformed into ether forms, resulting in the synthesis of **DHP-L6** (**3**) with a high yield of 87%. The ^{1}H NMR analysis of the product revealed peaks at 6.9−7.1 ppm (corresponding to the aromatic proton of **DHP**), 2.13 ppm (corresponding to a methyl group), and 6.02 ppm (attributed to a proton within the fluoroalkyl ether chain) (Figure S6). The successful synthesis of **DHP-L6** was also confirmed through ^{19}F and ^{13}C NMR analyses (Figures S7 and S8). The T_d of **DHP-L6** was determined to be 360 °C, indicating excellent thermal stability (Figure S9). However, no glass transition temperature was detected in DSC measurements, and only the isotropization

https://doi.org/10.1021/acsomega.4c05535
ACS Omega 2024, 9, 37365−37373

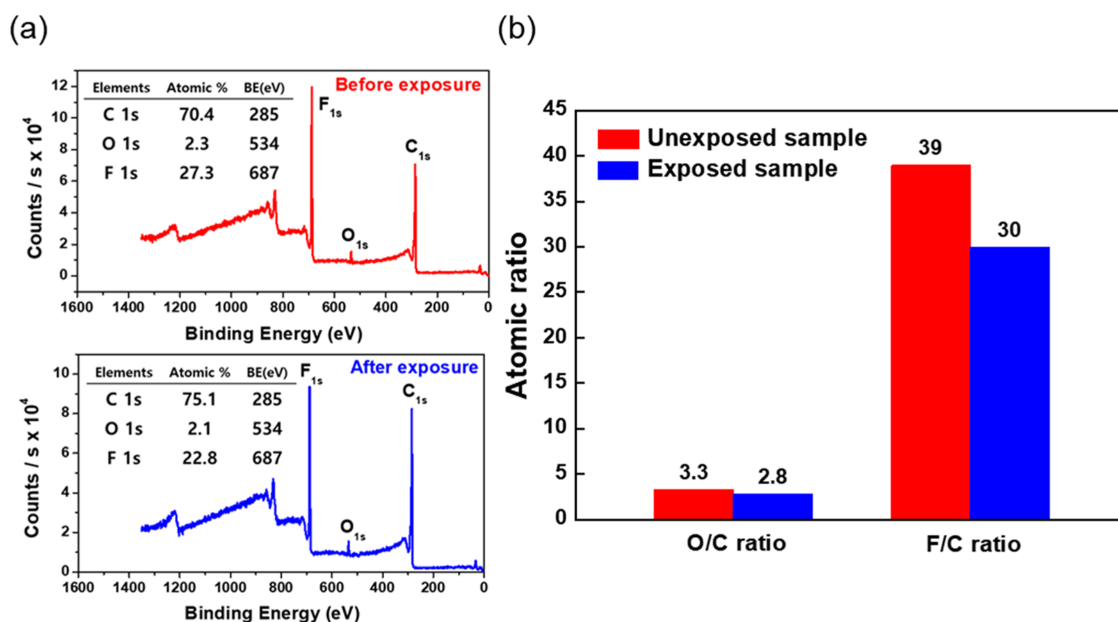

Figure 3. (a) XPS survey scans of **DHP-L6** films before and after EUV irradiation (100 mJ cm^{-2}). (b) Changes in O/C and F/C atomic ratios.

temperature (T_i) was observed around 140 °C (Figure S10).[40−42]

3.2. Analysis of Solubility Changes in DHP-L6 Films under EUV and E-Beam Irradiation.

The successful synthesis of **DHP-L6** prompted its evaluation as a potential e-beam and EUV resist. Initially, we assessed the performance of the film coating, followed by experiments aimed to observe changes in solubility under e-beam and EUV irradiation. A coating solution was prepared by dissolving **DHP-L6** at a concentration of 10% (wt/vol) in a fluorous solvent, Novec-7500. **DHP-L6** exhibits good solubility in organic solvents such as propylene glycol monomethyl ether acetate (PGMEA) and 2-heptanone, commonly used as resist coating solvents, but has poor solubility in propylene glycol monomethyl ether (PGME). However, when PGMEA and 2-heptanone were used as coating solvents, the coating process did not work well, requiring the use of fluorinated solvents (Figure S11). This solution in Novec-7500 was then spin-coated onto a Si substrate that had not been primed with hexamethyldisilazane (HMDS). The coated thin film had a thickness of approximately 300 nm. The XRD pattern obtained for this film revealed its amorphous nature (Figure S12).[43]

A **DHP-L6** film was exposed to a circular EUV beam with energy ranging from 10 to 250 mJ cm^{-2}. Given that the film can be dissolved in highly fluorinated solvents, such as FC-770 and FC-3283, with the latter proving more advantageous in enhancing sensitivity characteristics, the EUV-exposed film was developed using FC-3283. It was observed that the areas exposed to EUV light lost their solubility, resulting in the formation of a circular patch with a diameter of 220 μm (Figure 2a). Additionally, evaluations under e-beam lithography conditions confirmed that the e-beam also reduced the solubility of the **DHP-L6** film, thus enabling pattern formation (Figure S13a). The detailed methods and results of the e-beam irradiation experiments are available in the Supporting Information. The pattern formation under EUV and e-beam irradiation demonstrates that high-energy radiation induces chemical changes in the molecular structure of **DHP-L6**, leading to changes in solubility.

To investigate the chemical mechanisms behind the solubility changes in **DHP-L6** films under EUV and e-beam irradiation, we obtained FT-IR spectra showing the molecular structure of the film samples (Figure 2b). The spectra were recorded for a pristine film not exposed to EUV light, as well as films exposed to EUV irradiation with 110 and 250 mJ cm^{-2} energy. No significant differences were observed in the 1300−1160 cm^{-1} range, which corresponds to C−F and C−O−C bond stretching vibrations.[44,45] Similar results were observed for films exposed to e-beam irradiation (Figure S13b). These results suggest that the decrease in solubility of the **DHP-L6** films may be due to limited changes in the molecular structure of **DHP-L6**, rather than to extensive chemical transformations.

XPS analysis was performed to obtain deeper insights into changes in the elemental composition within the EUV-exposed **DHP-L6** films (Figure 3a). To avoid inaccurate results due to surface contamination, the surface was cleaned with Ar plasma for 15 s before analysis. A comparison of the atomic compositions of the pristine film and of those exposed to 100 mJ cm^{-2} EUV light showed a decrease in the contents of O and F relative to C upon exposure (Figure 3b). This trend was also observed in the films before and after e-beam irradiation (Figure S14). The observed decrease in the F to C ratio supports the hypothesis that defluorination is induced by the high-energy radiation. Additionally, a slight decrease was observed in the O/C atomic ratio, suggesting that moieties containing O atoms from the perfluoroalkyl ether chains are cleaved during exposure and subsequently volatilized from the film. Based on the observed decreases in F and O contents in **DHP-L6**, it can be speculated that the chemical mechanisms behind the solubility change of **DHP-L6** under EUV or e-beam irradiation involve the formation of intermolecular cross-links and a decrease in fluorine content caused by the cleavage of perfluoroalkyl moieties.

To further confirm the possibility of intermolecular cross-link formation within the **DHP-L6** films, the mechanical properties of the films before and after EUV exposure were examined using a nanoindentation technique. Figure 4 shows the hardness and reduced Young's modulus of **DHP-L6** films

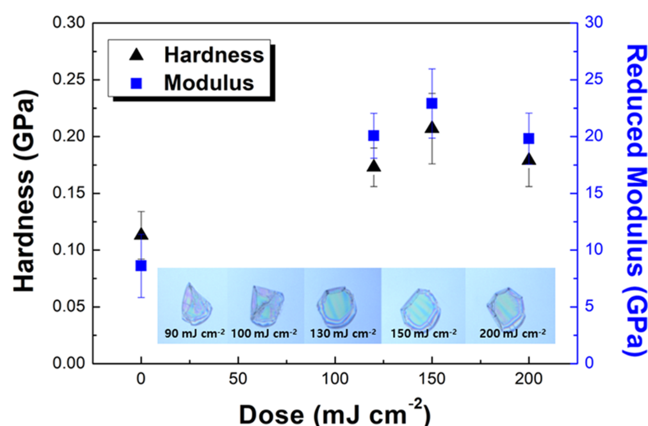

Figure 4. Hardness and reduced Young's modulus values of **DHP-L6** patches (inset photographs) generated by EUV light exposure with increasing doses and development process using FC-3283.

exposed to EUV energies of 130−200 mJ cm^{-2}. The films exhibited an increased hardness compared to that of the pristine sample before EUV exposure, which is attributed to the cross-linking reactions between the perfluoroalkyl ether chains of the **DHP-L6** molecules. Additionally, the reduced Young's modulus of the films after exposure to EUV light was found to be approximately twice that before exposure. These changes are also attributed to the intermolecular cross-linking of **DHP-L6**.[46,47] The same experiments were conducted on films exposed to e-beam irradiation (Figure S15). Nanoindentation measurements of films exposed to e-beam doses ranging from 300 to 1300 μC cm^{-2} revealed an increase in both hardness and reduced Young's modulus. Based on these results, it can be inferred that the formation of cross-links among the perfluoroalkyl ether moieties significantly contributes to the solubility decrease behavior of **DHP-L6** films under EUV or e-beam irradiation. The flexible nature of the perfluoroalkyl ether moieties in **DHP-L6** likely enhances the cross-linking reactions between the liberated fluoroalkyl radicals by increasing the possibility of their encounters.[48]

3.3. Lithographic Patterning Evaluation under E-Beam and EUV Irradiation. Before evaluating the lithographic patterning capability of **DHP-L6** using an EUV lithography tool with highly limited access opportunities, the performance was first tested using e-beam lithography. A 100 nm-thick film was exposed to an e-beam and developed using FC-3283, and the remaining patterns were observed using FE-SEM. The results showed that patterns of 100 and 70 nm were formed at an e-beam dose of 1000 μC cm^{-2}, while a 50 nm negative pattern was formed at 1100 μC cm^{-2} (Figure S16). This preliminary evaluation by e-beam lithography provides valuable insights for the subsequent assessment using EUV lithography.

Finally, the micropatterning performance of **DHP-L6** was evaluated under EUV lithography conditions. The experiments

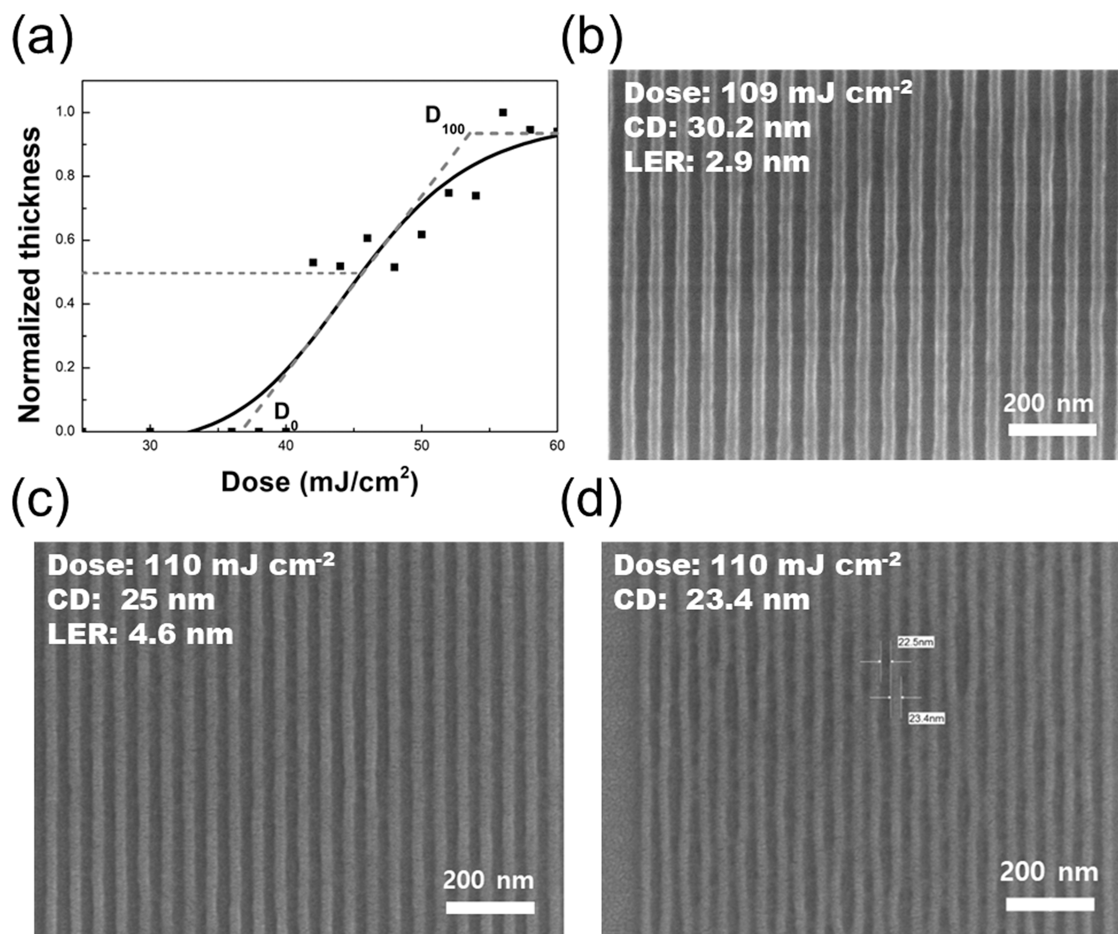

Figure 5. (a) Plot showing the solubility change behavior (contrast curve) of 40 nm-thick DHP-L6 films with increasing EUV doses; SEM images of (b) 30 nm, (c) 25 nm and (d) 23 nm half-pitch patterns of DHP-L6 film formed under EUV irradiation.

utilized the MET5 tool at LBNL. First, a 40 nm-thick film was exposed to a circular EUV beam with varying exposure doses to estimate the required energy for fine patterning. It was observed that, at approximately 45 mJ cm^{-2}, half of the original film thickness remained after washing in FC-3283. At exposure doses greater than 55 mJ cm^{-2}, ca. 90% of the coated film thickness was retained on the substrate. The D_0 and D_{100} values, representing the maximum dose required for complete removal of the resist film and the minimum dose for retaining the maximum film thickness, were estimated as shown in Figure 5a. D_0 and D_{100} were determined to be 36.9 and 53.6 mJ cm^{-2}, respectively. With these values, the contrast [$\gamma = 1/\log(D_{100}/D_0)$] could be calculated to be 6.2.[49]

Based on our previous experience, we could select the EUV exposure dose range, because lithographic patterning requires at least twice this amount of energy. Subsequently, fine patterns were printed on the **DHP-L6** film using a photomask. After development with FC-3283, the patterns were examined using FE-SEM. To facilitate the observation, the sample surface was coated with conductive Os using CVD. The results revealed that for 30 nm-sized half-pitch patterns created with an exposure energy of 109 mJ cm^{-2}, the LER was measured to be as low as 2.9 nm. It was confirmed that negative-tone half-pitch patterns with a line width of 25 nm and a LER of 4.6 nm were formed at an exposure energy of 110 mJ cm^{-2} (Figure 5b,c). The power spectral density curves for these patterns obtained using SUMMIT software are presented in Figure S17. However, pattern collapse was observed in the 23 nm-sized half-pitch patterns (Figure 5d). These results show that single-component molecular materials containing perfluoroalkyl moieties can be effectively employed as resists under EUV and e-beam irradiation. However, the results also highlight the need for a relatively high exposure energy to achieve high-resolution patterns and the difficulty in forming high-resolution patterns below 20 nm, suggesting that further research is required to optimize the performance of these materials for practical applications.

4. CONCLUSIONS

A potential EUV resist, **DHP-L6**, was synthesized by incorporating six fluoroalkyl ether chains into amorphous and high-T_g **DHP**. The film cast using **DHP-L6** was confirmed to be amorphous. After exposing the **DHP-L6** films to EUV and e-beam irradiation, we observed a negative-tone patterning behavior characterized by reduced solubility in the exposed areas. The exploration of the chemical mechanisms behind this phenomenon using FT-IR, XPS, and nanoindentation techniques revealed that C−F bonds decompose under electron injection conditions, leading to the formation of C-centered radicals. These radicals bind to each other, resulting in the solubility decrease. Subsequent high-resolution lithographic patterning experiments under EUV irradiation revealed that a minimum line width of 26 nm could be achieved with an exposure dose of 110 mJ cm^{-2}, and patterns of 30 nm size exhibited a LER of 2.9 nm. These results confirm that single-component molecular materials containing perfluoroalkyl moieties can serve as effective resist systems under ionizing radiation, including EUV and e-beam sources.

■ ASSOCIATED CONTENT

Supporting Information

The Supporting Information is available free of charge at https://pubs.acs.org/doi/10.1021/acsomega.4c05535.

Structure of fluorous solvents (Novec-7500, FC-3283, FC-770, FC-40, Novec-7600); structure of CYTOP, Hyflon AD, and Teflon AF with SEM images of e-beam lithographic patterns; synthesis, TGA, DSC curves, and NMR spectra (^{1}H, ^{19}F, ^{13}C); solubility and coating tests; X-ray diffraction pattern of film; e-beam lithography; exploration of working mechanism under e-beam irradiation (ATR FT-IR, XPS and nanoindentation); SEM images of patterns under various e-beam doses (PDF)

■ AUTHOR INFORMATION

Corresponding Author

Jin-Kyun Lee − *Department of Polymer Science and Engineering, Inha University, Incheon 22212, Republic of Korea; Program in Environmental and Polymer Engineering, Inha University, Incheon 22212, Republic of Korea;* orcid.org/0000-0001-9468-5749; Email: jkl36@inha.ac.kr

Authors

Hyun-Taek Oh − *Department of Polymer Science and Engineering, Inha University, Incheon 22212, Republic of Korea*

Gayoung Kim − *Program in Environmental and Polymer Engineering, Inha University, Incheon 22212, Republic of Korea*

Seok-Heon Jung − *Department of Polymer Science and Engineering, Inha University, Incheon 22212, Republic of Korea*

Yejin Ku − *Program in Environmental and Polymer Engineering, Inha University, Incheon 22212, Republic of Korea*

Kanghyun Kim − *Department of Mechanical Engineering, POSTECH, Pohang 37673, Republic of Korea*

Byeong-Gyu Park − *Pohang Accelerator Laboratory, POSTECH, Pohang 37673, Republic of Korea*

Sangsul Lee − *Pohang Accelerator Laboratory, POSTECH, Pohang 37673, Republic of Korea*

Chawon Koh − *Samsung Electronics Co., Ltd., Semiconductor R&D Center, Suwon 18448, Republic of Korea; Department of Materials Science and Engineering, Yonsei University, Seoul 03722, Republic of Korea*

Tsunehiro Nishi − *Samsung Electronics Co., Ltd., Semiconductor R&D Center, Suwon 18448, Republic of Korea*

Hyun-Woo Kim − *Samsung Electronics Co., Ltd., Semiconductor R&D Center, Suwon 18448, Republic of Korea*

Complete contact information is available at: https://pubs.acs.org/10.1021/acsomega.4c05535

Author Contributions

[∇]H.-T.O. and G.K. contributed equally to this work. The manuscript was written through contributions of all authors. All authors have given approval to the final version of the manuscript.

Notes

The authors declare no competing financial interest.

■ ACKNOWLEDGMENTS

This study was funded by the Samsung Research Funding & Incubation Center for Future Technology (Project Nos. SRFC-TA1703-05 and SRFC-TA1703-51). The authors also acknowledge the Samyang Yangyoung Foundation for its financial assistance on academic research.

■ REFERENCES

(1) Kilby, J. S. C. Turning potential into realities: The invention of the integrated circuit (Nobel lecture). *ChemPhysChem* **2001**, *2* (8−9), 482−489.

(2) O'Regan, G. Integrated Circuit and Silicon Valley. In *A Brief History of Computing*; Springer, 2021; pp 89−96.

(3) Pease, R. F. Imprints offer moore. *Nature* **2002**, *417* (6891), 802−803.

(4) Mack, C. *Fundamental Principles of Optical Lithography: the Science of Microfabrication*; John Wiley & Sons, 2007.

(5) Lio, A. EUV photoresists: A progress report and future prospects. *Synchrotron Radiat. News* **2019**, *32* (4), 9−14.

(6) Naulleau, P. EUV lithography patterning challenges. *Front. Nanosci.* **2016**, *11*, 177−192.

(7) Bruning, J. H.*Optical Lithography: 40 Years and Holding*, Optical Microlithography XX (SPIE); SPIE, 2017; pp 62−74.

(8) Brainard, R. L.; Trefonas, P.; Lammers, J. H.; Cutler, C. A.; Mackevich, J. F.; Trefonas, A.; Robertson, S. A. In *Shot Noise, LER, and Quantum Efficiency of EUV Photoresists*, Emerging Lithographic Technologies VIII (SPIE); SPIE, 2004; pp 74−85.

(9) Hutchinson, J. M. In *Shot-Noise Impact on Resist Roughness in EUV Lithography*, Emerging Lithographic Technologies II (SPIE); SPIE, 1998; pp 531−536.

(10) Levinson, H. J. High-NA EUV lithography: current status and outlook for the future. *Jpn. J. Appl. Phys.* **2022**, *61* (SD), No. SD0803.

(11) Manouras, T.; Kazazis, D.; Ekinci, Y. In *Chemically-Amplified Backbone Scission (CABS) Resist for EUV Lithography*, Extreme Ultraviolet (EUV) Lithography XII (SPIE); SPIE, 2021; pp 24−32.

(12) Pawloski, A. R.; Christian; Nealey, P. F. The multifunctional role of base quenchers in chemically amplified photoresists. *Chem. Mater.* **2002**, *14* (10), 4192−4201.

(13) Ito, H.Chemical Amplification Resists for Microlithography. In *Microlithography Molecular Imprinting*; Springer, 2005; pp 37−245.

(14) Nishikori, K.; Kasahara, K.; Kaneko, T.; Sakurai, T.; Dei, S.; Maruyama, K.; Ayothi, R. In *Stochastic Effects on EUV CAR Systems: Investigation of Materials Impact*, Advances in Patterning Materials and Processes XXXVII (SPIE); SPIE, 2020; pp 185−190.

(15) Kaefer, F.; Yuan, C.; Adams, C.; Segalman, R.; Ober, C. K. Photoresist Design to Address Stochastics Issues in EUV Resists. *J. Photopolym. Sci. Technol.* **2023**, *36* (1), 61−66.

(16) Schmid, G. M.; Stewart, M. D.; Wang, C.-Y.; Vogt, B. D.; Prabhu, V. M.; Lin, E. K.; Willson, C. G. In *Resolution Limitations in Chemically Amplified Photoresist Systems*, Advances in Resist Technology and Processing XXI (SPIE) SPIE, 2004; pp 333−342.

(17) De Silva, A.; Felix, N. M.; Ober, C. K. Molecular Glass Resists as High-Resolution Patterning Materials. *Adv. Mater.* **2008**, *20* (17), 3355−3361.

(18) Peng, X.; Wang, Y.; Xu, J.; Yuan, H.; Wang, L.; Zhang, T.; Guo, X.; Wang, S.; Li, Y.; Yang, G. Molecular glass photoresists with high resolution, low LER, and high sensitivity for EUV lithography. *Macromol. Mater. Eng.* **2018**, *303* (6), No. 1700654.

(19) Wang, Y.; Chen, L.; Yu, J.; Guo, X.; Wang, S.; Yang, G. Negative-tone molecular glass photoresist for high-resolution electron beam lithography. *R. Soc. Open Sci.* **2021**, *8* (3), No. 202132.

(20) Chen, J.; Hao, Q.; Wang, S.; Li, S.; Yu, T.; Zeng, Y.; Zhao, J.; Yang, S.; Wu, Y.; Xue, C.; et al. Molecular glass resists based on 9, 9′-spirobifluorene derivatives: pendant effect and comprehensive evaluation in extreme ultraviolet lithography. *ACS Appl. Polym. Mater.* **2019**, *1* (3), 526−534.

(21) Hu, S.; Chen, J.; Yu, T.; Zeng, Y.; Yang, G.; Li, Y. Chemically Amplified Resist Based on Dendritic Molecular Glass for Electron Beam Lithography. *Chem. Res. Chin. Univ.* **2023**, *39* (1), 139−143.

(22) Wang, Y.; Yuan, J.; Chen, J.; Zeng, Y.; Yu, T.; Guo, X.; Wang, S.; Yang, G.; Li, Y. A Single-Component Molecular Glass Resist Based on Tetraphenylsilane Derivatives for Electron Beam Lithography. *ACS Omega* **2023**, *8* (13), 12173−12182.

(23) Wang, Y.; Chen, J.; Zeng, Y.; Yu, T.; Wang, S.; Guo, X.; Hu, R.; Tian, P.; Vockenhuber, M.; Kazazis, D.; et al. Nonchemically Amplified Molecular Resists Based on Sulfonium-Functionalized Sulfone Derivatives for Sub-13 nm Nanolithography. *ACS Appl. Nano Mater.* **2023**, *6* (19), 18480−18490.

(24) Kim, K.; Lee, J.-W.; Park, B.-G.; Oh, H.-T.; Ku, Y.; Lee, J.-K.; Lim, G.; Lee, S. Investigation of correlative parameters to evaluate EUV lithographic performance of PMMA. *RSC Adv.* **2022**, *12* (5), 2589−2594.

(25) Blackborow, P. A.; Partlow, M. J.; Horne, S. F.; Besen, M. M.; Smith, D. K.; Gustafson, D. S. In *EUV Source Development at Energetiq*, Emerging Lithographic Technologies XII (SPIE); SPIE, 2008; pp 622−632.

(26) Kostko, O.; McAfee, T. R.; Naulleau, P. In *Experimental Characterization of EUV Resist Materials: Photoelectron Spectroscopy*, Advances in Patterning Materials and Processes XXXIX (SPIE); SPIE, 2022; pp 49−56.

(27) Ma, J. H.; Wang, H.; Prendergast, D.; Neureuther, A.; Naulleau, P. In *Investigating EUV Radiation Chemistry with First Principle Quantum Chemistry Calculations*, International Conference on Extreme Ultraviolet Lithography 2019 (SPIE); SPIE, 2019; pp 103−113.

(28) Belmonte, G. K.; da Silva Moura, C. A.; Reddy, P. G.; Gonsalves, K. E.; Weibel, D. E. EUV photofragmentation and oxidation of a polyarylene−Sulfonium resist: XPS and NEXAFS study. *J. Photochem. Photobiol., A* **2018**, *364*, 373−381.

(29) Chambers, R. D. *Fluorine in Organic Chemistry*; CRC Press, 2004.

(30) O'Hagan, D. Understanding organofluorine chemistry. An introduction to the C−F bond. *Chem. Soc. Rev.* **2008**, *37* (2), 308−319.

(31) Oshima, A.; Ikeda, S.; Seguchi, T.; Tabata, Y. Change of molecular motion of polytetrafluoroethylene (PTFE) by radiation induced crosslinking. *Radiat. Phys. Chem.* **1997**, *49* (5), 581−588.

(32) Adhi, K. P.; Owings, R. L.; Railkar, T. A.; Brown, W.; Malshe, A. Femtosecond ultraviolet (248 nm) excimer laser processing of Teflon (PTFE). *Appl. Surf. Sci.* **2003**, *218* (1−4), 17−23.

(33) Blakey, I.; George, G. A.; Hill, D. J.; Liu, H.; Rasoul, F.; Rintoul, L.; Zimmerman, P.; Whittaker, A. K. Mechanism of 157 nm photodegradation of poly [4, 5-difluoro-2, 2-bis (trifluoromethyl)-1, 3-dioxole-co-tetrafluoroethylene](Teflon AF). *Macromolecules* **2007**, *40* (25), 8954−8961.

(34) Popovici, D.; Sacher, E.; Meunier, M. Photodegradation of Teflon AF1600 during XPS analysis. *J. Appl. Polym. Sci.* **1998**, *70* (6), 1201−1207.

(35) Forsythe, J. S.; Hill, D. J.; Logothetis, A. L.; Whittaker, A. K. The radiation chemistry of the copolymer of tetrafluoroethylene with 2, 2-bis (trifluoromethyl)-4, 5-difluoro-1, 3-dioxole. *Polym. Degrad. Stab.* **1999**, *63* (1), 95−101.

(36) Oh, H.-T.; Jung, S.-H.; Kim, K.-H.; Moon, Y.; Jeong, D. H.; Ku, Y.; Lee, S.; Park, B.-G.; Lee, J.; Koh, C.; et al. Perfluoroalkylated alternating copolymer possessing solubility in fluorous liquids and imaging capabilities under high energy radiation. *RSC Adv.* **2021**, *11* (3), 1517−1523.

(37) Mun, J.-S.; Woo, J.-H.; Ku, Y.; Oh, H.-T.; Lee, J. H.; Lee, J.-K.; Kim, K.; Park, B.-G.; Lee, S. Dendritic Polyphenol with an Improved Glass Transition Temperature for Microelectronic Applications. *ACS Mater. Lett.* **2023**, *5* (4), 1164−1169.

(38) Ku, Y.; Kim, K.; Oh, H.-T.; Park, B.-G.; Lee, S.; Lee, J.-K.; Koh, C.; Nishi, T.; Kim, H.-W. Extreme UV Resist Exhibiting Synergism between Chemical and Physical Crosslinking Mechanisms. *Langmuir* **2023**, *39* (9), 3462−3470.

https://doi.org/10.1021/acsomega.4c05535
ACS Omega 2024, 9, 37365−37373

(39) Young, R. J.; Lovell, P. A. *Introduction to Polymers*; CRC Press, 2011; p 138.
(40) Galli, G.; Ragnoli, M.; Bertolucci, M.; Ober, C.; Kramer, E.; Chiellini, E. Fluorinated 2-Vinylcyclopropane Copolymers as Low Surface Energy Materials. *Macromol. Symp.* **2004**, *218*, 303−312.
(41) Ishige, R.; Shinohara, T.; White, K. L.; Meskini, A.; Raihane, M.; Takahara, A.; Ameduri, B. Unique difference in transition temperature of two similar fluorinated side chain polymers forming hexatic smectic phase: poly {2-(perfluorooctyl) ethyl acrylate} and poly {2-(perfluorooctyl) ethyl vinyl ether}. *Macromolecules* **2014**, *47* (12), 3860−3870.
(42) Orodepo, G. O.; Gowd, E. B.; Ramakrishnan, S. Main-chain liquid crystalline polymers bearing periodically grafted folding elements. *Polym. Chem.* **2021**, *12* (7), 1050−1059.
(43) Xu, H.; Sakai, K.; Kasahara, K.; Kosma, V.; Yang, K.; Herbol, H. C.; Odent, J.; Clancy, P.; Giannelis, E. P.; Ober, C. K. Metal−organic framework-inspired metal-containing clusters for high-resolution patterning. *Chem. Mater.* **2018**, *30* (12), 4124−4133.
(44) Lim, M.-Y.; Kim, K. Sulfonated poly (arylene ether sulfone) and perfluorosulfonic acid composite membranes containing perfluoropolyether grafted graphene oxide for polymer electrolyte membrane fuel cell applications. *Polymers* **2018**, *10* (6), No. 569.
(45) Bentel, M. J.; Yu, Y.; Xu, L.; Kwon, H.; Li, Z.; Wong, B. M.; Men, Y.; Liu, J. Degradation of perfluoroalkyl ether carboxylic acids with hydrated electrons: structure−reactivity relationships and environmental implications. *Environ. Sci. Technol.* **2020**, *54* (4), 2489−2499.
(46) Hartl, H.; East, C.; Xu, Y.; Yambem, S. D.; Fairfull-Smith, K. E.; MacLeod, J. Direct-write crosslinking in vacuum-deposited small-molecule films using focussed ion and electron beams. *Nanotechnology* **2019**, *30* (33), No. 335301.
(47) Park, K.; Mishra, S.; Lewis, G.; Losby, J.; Fan, Z.; Park, J. B. Quasi-static and dynamic nanoindentation studies on highly cross-linked ultra-high-molecular-weight polyethylene. *Biomaterials* **2004**, *25* (12), 2427−2436.
(48) Hill, D. J.; Whittaker, A. K.Radiation Chemistry of Polymers. In *Encyclopedia of Polymer Science and Technology*; Wiley, 2002; p 27.
(49) Valdez, M.; Joshi-Imre, A.; Bonner, J. C.; Preimesberger, L. Z.; Grayson, J. L.; Hsu, J. W. In *Indium Nitrate Hydrate Resist Characteristics Evaluated by Low-Energy Electron Beam Exposure*, Advances in Patterning Materials and Processes XLI (SPIE); SPIE, 2024; pp 120−129.

https://doi.org/10.1021/acsomega.4c05535
ACS Omega 2024, 9, 37365−37373